Forensic Science International 295 (2019) 189–198

Contents lists available at ScienceDirect

Forensic Science International

journal homepage: www.elsevier.com/locate/forsciint

Surface coatings including fingerprint residues can significantly alter the size and shape of bloodstains

Samira Shiri[a], Kenneth F. Martin[b], James C. Bird[a,*]

[a] Department of Mechanical Engineering, Boston University, Boston, MA 02215, USA
[b] Biomedical Forensic Sciences, Graduate Medical Sciences, Boston University School of Medicine, Boston, MA 02118, USA

ARTICLE INFO

Article history:
Received 8 June 2018
Received in revised form 6 November 2018
Accepted 10 December 2018
Available online 19 December 2018

Keywords:
Bloodstain pattern analysis
Surface coating
Human blood drop impact
Drying
Terminal velocity
Clotting

ABSTRACT

When conducting a blood pattern analysis (BPA) the size, shape, distribution, and location of bloodstains found at a crime scene may be critical in forming a hypothesis as to what transpired during a bloody event. Prior studies have demonstrated that the size and shape of a bloodstain on a smooth surface are determined from impact dynamics and to a lesser degree by the target material itself. Yet, these studies have relied on clean surfaces, and it is unclear whether the presence of microscopic coatings and residues could significantly alter the size or shape of the dried stain. Here, in the present work, experiments are conducted to demonstrate that various coatings, such as the sebaceous residue from a latent fingerprint, can dramatically alter the size and shape of the stain from the moment of impact through the drying process. These experiments also highlight that a drop impacting a tilted superhydrophobic-coating glass substrate can cause the blood drop to completely recoil without leaving a stain. Relying on a combination of high-speed and time-lapse photography, the specific stages in the stain evolution responsible for the deviations from the current models are identified. At a relatively low impact velocity, the stain sizes on the coated glass surfaces were 35–72% smaller than on the clean glass surface. At a higher impact velocity, the stains on the coated surfaces were not only smaller, but also contained drop spatter around the primary stain that was not observable in the absence of the microscopic coatings. The reduction in bloodstain size did not appreciably change when a chemical was added to deactivate the anticoagulant and allow the blood to clot.

1. Introduction

For over a century, blood pattern analysis (BPA) has been used by forensic scientists with the intention of reconstructing crime scenes [1–8] using the evidence in court to either provide missing details or to challenge or support a witness's testimony. In situations where blood spatter is present, the size of blood stains are often associated with the force involved, whereas the shape and location of the stains can provide insight into an approximate area of origin [9]. Here detectives use a stringing technique to find a region of origin by assuming blood drops follow straight lines [10], an assumption that can overestimate the height by tens of centimeters [11,8]. Within the last decade, methods have been developed to back out the in-flight parabolic trajectories of the drops that account for gravitational and drag effects [12]. To apply these methods, accurate estimate for the initial drop size and impact velocity are required.

Numerous studies have been carried out to relate the drop size and impact velocity to the final size and shape of bloodstain [13–17]. These studies typically relate impact conditions with the number of spines radiating from the dried drop [13] or—in the absence of spines—with the stain size itself [15]. These relations appear to depend predominantly on the impact conditions [16], with some corrections based on the target properties [14,17]. Thus, under the same impact conditions, the bloodstain size might differ if the target were glass as opposed to polycarbonate. It is noteworthy that in almost all experiments investigating bloodstains, the target is cleaned before impact. However, at a crime scene, a surface may have unknown coatings or contaminants which may be invisible to the eye. For example, a window pane may be coated with fingerprints, a kitchen counter with a microscopic layer of oil, or a storefront with commercially-available, superhydrophobic, anti-graffiti paint [18]. Here, a natural question arises: can the presence of microscopic coatings fundamentally alter the size or shape of the dried stain?

This study investigates the effect of microscopic coatings on the final bloodstain size and shape from the vertical impact of a single drop of human blood. Coatings used here include natural

* Corresponding author.
E-mail address: jbird@bu.edu (J.C. Bird).

https://doi.org/10.1016/j.forsciint.2018.12.008
0379-0738/

secretions deposited as fingerprints, vegetable oil, and a superhydrophobic coating. Experiments were conducted at impact velocities both below and above values when splashing might be expected to occur. The study also explored the influence of clotting in the final stain formation. In all experiments, high-speed and time-lapse photography were combined to document the influence of the coatings from the first milliseconds of impact to the final hours of drying. The experimental findings are contrasted with existing models to highlight that caution should be used when conducting bloodstain pattern analysis on surfaces that might be coated or contaminated.

2. Material and methods

To test effect of microscopic coatings on a bloodstain size and shape, systematic experiments were conducted in a laboratory environment. In these experiments, different coatings were prepared on glass slides as outlined in Section 2.1. Drops of blood impacted each of these surfaces. Section 2.2 reports the physical properties of the human blood used in the experiments. The blood contained anticoagulants to prevent clotting between experiments. To see influence of clotting on the bloodstain pattern, in some experiments the anticoagulant was deactivated following the protocol outlined in Section 2.3.

The drop impact setup and procedure are described in Section 2.4. In each experiment, a single human blood drop was released onto one of the prepared glass slides from a fixed height to set the impact velocity. By imaging the drop with both high-speed and time-lapse photography, the drop dynamics leading to the final stain were measured and quantified.

2.1. Surface preparation

Five different sets of surfaces were used in this study, all starting with cleaned glass slides (VWR® Plain Micro Slides). The first set of glass slides was cleaned and left uncoated to be used as a control. To ensure there were no pre-existing oils or organic residues, a three-solvent method was used. In this method, the glass slide was first rinsed with acetone, then with isopropanol, and finally with methanol, after which it was dried with pressurized air. These slides are referred to as 'clean'.

The second set of glass slides was coated with the natural secretions from a fingerprint by a finger tapping across the slide. The commission of a crime can present an extremely stressful situation for many individuals, resulting in excessive sweating [19]. This situation may lead a suspect to deposit enough secretions to form a comprehensive surface coating with minimal contact. The coated surfaces were viewed under oblique lighting to confirm the residue was present.

The third set of surfaces were partially coated with fingerprint residue to create a binary surface, referred henceforth as a 'half clean–half fingerprint' coating. To prepare this coating, a glass slide is first cleaned with solvents. Half of the slide is then covered with Scotch tape to serve as a mask and the edge of the tape is identified on the reverse side of the slide with permanent ink. Natural secretions that form fingerprints are deposited onto the masked slide by repeatedly tapping a finger along the surface. When the tape is subsequently removed, there is a sharp boundary between the portion of the glass that has been exposed to fingerprint secretion and the portion that has not. The tape does not appear to leave a residue when it is removed from the glass; indeed this clean removal has been documented in the microdevice fabrication literature [20].

The forth set of glass slides was coated with vegetable oil. To create a thin uniform coating, 50 μL of vegetable oil was deposited on a clean glass slide with a micropipette. A second clean glass slide was placed over the oil, and the slides were translated relative to one another to promote a uniform coverage of the oil. When the slide were separated, conservation of mass suggests that both were slides were coated with a 5–10μm-thick layer of vegetable oil.

The fifth set of target substrates consisted of a commercially-available superhydrophobic coating (Ultra-Ever Dry®) applied to glass slides. By definition, superhydrophobic surfaces combine chemical hydrophobicity with micro/nano-textured roughness. This roughness can trap air to create a surface that is so hydrophobic that impacting water drops contact the surface and rapidly bounce off [21,22]. Both a bottom and top coat were applied on to cleaned glass slides, and once fully dried, water drops were placed on the surface to ensure the coating was superhydrophobic.

2.2. Human blood characterization

Many recent blood impact studies have relied on swine blood [13,7,17]. However when drawing inferences to bloodstains in crime scenes, using human blood is preferable [23,24]. In the current experiments, whole human blood is drawn and certified by a third-party company (Lampire Biological Laboratories) with a standard sodium citrate anticoagulant. All experiments and measurements were performed within one week of the blood being drawn, and no signs of degradation were apparent.

The fresh human blood was stored in a refrigerator at 5 °C. Prior to conducting each set of experiments, the blood was placed in a water bath set at 37 °C to approximate human body temperature and stirred with a vortex mixer to ensure a uniform blood cell suspension.

Existing models for the impact dynamics of blood depend on the blood viscosity μ, density ρ, and surface tension γ and therefore representative values of these parameters needed to acquired [14,25]. The viscosity of blood depends on its temperature, as well as the volume fraction of red blood cells, often referred to as the hematocrit [26,27]. For the blood in this study, the hematocrit was approximately 47%, determined by directly measuring the blood cell sediments and comparing it to the total volume of blood. The viscosity of this blood at 37 °C was measured to be $\mu = 4.2$ mPa s. This representative measurement was obtained with a vibrational viscometer oscillating at a constant frequency of 30 Hz and amplitude of less than 1 mm. Although it is known that blood is a shear-thinning liquid, bloodstain experiments and models have indicated that accounting for this complex fluid behavior is generally unnecessary [17,24]. The role of temperature on blood viscosity has been documented [28]. For completeness, the blood viscosity is the current study is measured over a range of temperatures and plotted in Fig. 1a. Here the confidence at each temperature is indicated with a standard deviation σ above and below the mean. The other measured properties for the blood used in the experiments are tabulated in Fig. 1b. To find the density of the blood, blood samples were weighed at known volumes, resulting in a measured density of $\rho = 1021 \pm 8\ \mathrm{kg\,m^{-3}}$. The surface tension of the blood was measured to be $\gamma = 61.1 \pm 0.9\ \mathrm{mN\,m^{-1}}$ using a standard pendant drop method [29].

Another potentially important material property is the contact angle θ between the blood and the surface. For the oil-coated glass, the contact angle between the blood, oil, and air can be calculated precisely with Young's equation [30] since both the surface tension of the blood in air and the surface tension of oil in air can be measured independently. For the other coatings, the less precise, but reasonably accurate, sessile drop method is used [31].

2.3. Enabling blood to clot

Most of the experiments carried out in this study were conducted with the blood sample unaltered. However because

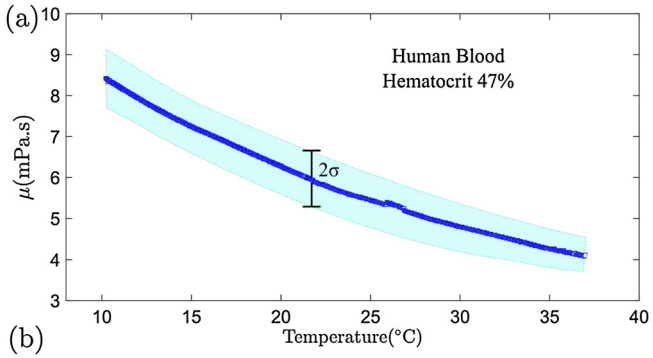

Density (ρ)	Surface tension (γ)	Contact angle (θ)			
		Clean glass	Fingerprint coated glass	Oil coated glass	Superhydrophobic coated glass
1021±8 Kg/m³	61.1±0.9 mN/m	15°	43°	79°	135°

Fig. 1. The properties of the Human blood used in the experiments. (a) The dynamic viscosity μ of the blood decreases with temperature. Repeated viscosity measurements for the sample, which had a hematocrit of 47%, were taken to calculate a standard deviation σ (shaded region). (b) A table illustrates the values of the blood density ρ, surface tension γ, and contact angles θ on the various surfaces.

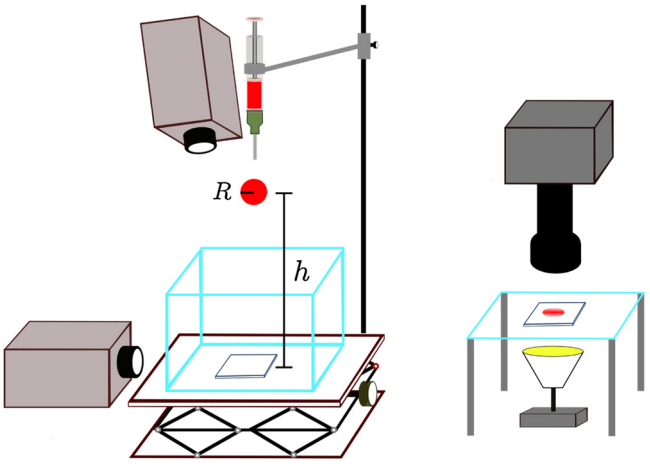

Fig. 2. Experimental setup. A blood drop of radius R is released from a syringe at height h above the target substrate. The dynamics were filmed simultaneously with two high-speed cameras at different vantage points. After impact, the sample was moved to a back-lit stand and was photographed every minute as it dried. In addition to the substrate coating, the size of drop R and release height h were varied between experiments.

this blood contains anticoagulant, the blood does not clot as it spreads and dries on the surface. To evaluate if clotting significantly effects bloodstain patterns on the tested coatings, experiments were also conducted with the anticoagulant deactivated. There are several possible chemicals that will act as an anticoagulant. In the current experiments, human blood with a sodium citrate anticoagulant was chosen, as it can be deactivated by adding a 1:59 ratio of 0.5 molar calcium chloride solution [32]. The material properties of this mixture are not expected to vary significantly from the properties of the blood itself. Measurements from pendent drop experiments indicate that the surface tension decreases to $\gamma = 60.7 \pm 0.9\,\mathrm{mN\,m^{-1}}$, a volume fraction calculation suggests that the density decreases to $\rho = 1020 \pm 8\,\mathrm{kg\,m^{-3}}$, and from Grunberg–Nissan mixing rule [33], the mixture viscosity is estimated to decrease to $\mu = 4.1$ mPa s.

2.4. Blood impact experiments

To explore the influence of the surface coatings on the final bloodstains, a series of drop impact experiments are carried out (Fig. 2). After the human blood was resuspended and warmed, it was placed into a syringe located at a height h above the prepared surface. The radius of the released drop was selected to be either $R = 1.0 \pm 0.1$ mm or $R = 2.0 \pm 0.1$ mm. This size was controlled with the diameter of the syringe needle, and because any dried blood on the needle might alter the drop size, a new needle was used before each experiment. Upon detaching from the needle, the drop would fall onto the target surface, accelerating under the influence of gravity. Impact velocity adjustments U were made by changing the height h at which drops were released.

The impact dynamics from a side perspective were captured with a high-speed camera (Photron SA-5) filming at 10 000 frames per second. From these images, the size R and velocity U could be calculated for each individual blood drop at the moment of impact. A second high-speed camera (Photron SA-X2) was synchronized to take simultaneous images from a top-down perspective (Fig. 2). The combination of vantage points allowed for a more complete measurement of the droplet shape as it impacted and spread along the surface, including measurements of processes that might break symmetry. Within a minute after impact, the sample was carefully moved to a back-lit platform, and images were captured every minute for three hours with a Nikon DSLR camera (Fig. 2).

3. Results and discussion

3.1. Bloodstains on clean glass

The results from the experiments on the clean glass are presented and discussed first, as bloodstains on these surfaces have been studied in the past [9] and can provide a baseline from which to evaluate the other surfaces. Blood drops of two sizes ($R = 1$ mm and 2 mm) were released from four heights: $h = 10$ cm, 20 cm, 100 cm, and 200 cm. The measured impact velocity ranged from $U = 1.5\,\mathrm{m\,s^{-1}}$ to $6.1\,\mathrm{m\,s^{-1}}$, consistent with gravitational acceleration resisted by air drag (Fig. 3a). Note that even when released from 200 cm, the drops are expected to be below their terminal velocity U_t when they impact the substrate. Terminal velocity can be estimated by balancing the weight of the drop and the drag force with the coefficient of drag approximated to be 0.47 (black lines on left-side of Fig. 3a). These terminal velocities are similar to what has been measured for rain drops [34].

Fig. 3b shows images of the blood stains that result from these blood drops after they impact and dry on the glass surface. Each bloodstain is circular with a final size r_f that depend on the initial size R and release height h. More generally, the final stain size on a given surface is considered to depend on the initial drop diameter $2R$, impact velocity U, density ρ, viscosity μ, and surface tension γ. Through dimensional analysis, the parameter space can be reduced such that the spreading factor $\beta = r_f/R$ depends only on two variables, the Reynolds number, $Re \equiv \rho U(2R)/\mu$ and the Weber number $We \equiv \rho(2R)U^2/\gamma$.

The results in Fig. 3b are consistent with several existing models, two of which are directly compared (Fig. 3c). The first expression [15] is based on an energy balance and predicts that for horizontal surfaces

$$\frac{r_f}{R} = \beta = \left(\frac{We + 12}{3(1 - \quad \cos \quad \theta) + 4We\,\mathrm{Re}^{-1/2}} \right)^{1/2}, \tag{1}$$

where θ is the equilibrium contact angle. Another expression [16] is written in terms of a Padé approximant, an approximation that is written in terms of a ratio of two power series. These series are advantageous in that they typically converge rapidly relative to other standard approximations, and therefore can be more

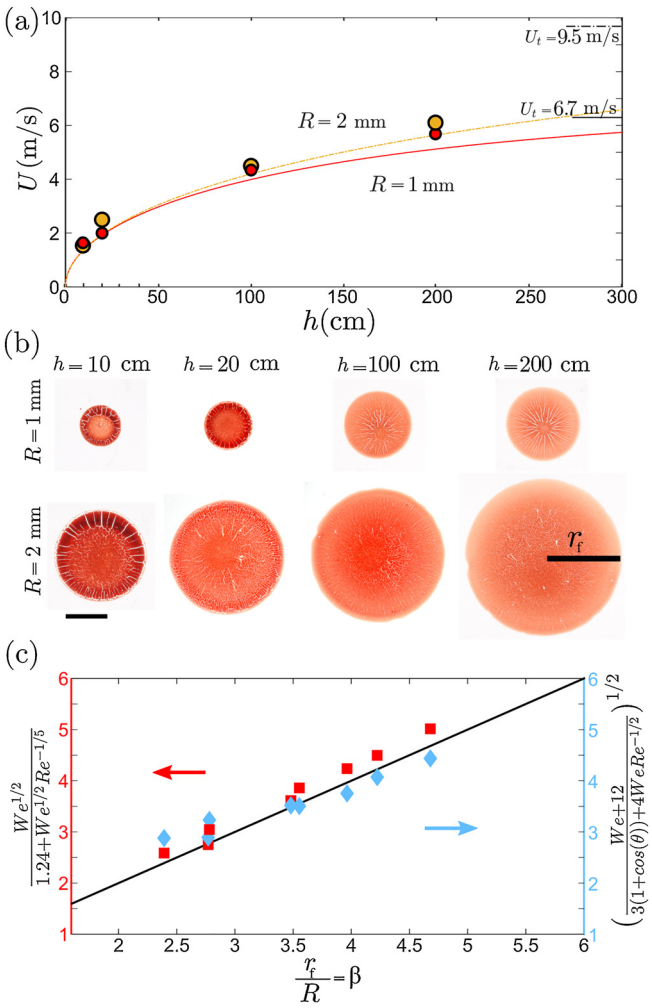

Fig. 3. Comparison of the size of dried human bloodstains on a clean glass surface with the published predictions. (a) The impact velocity U increases with release height h and drop size R. Theoretical predictions (curves) for drop sizes of $R = 1$ (small circles) and 2 mm (large circles) indicate that the drops in the experiments have not reached terminal velocity U_t. (b) The shape of the dried bloodstain on the glass surface is circular with a final size r_f that depends on the initial size R and release height h. The scalebar of 5 mm applies to all images. (c) The spreading factors $r_f/R = \beta$ for the experiments are plotted in terms of the dimensionless groups of Weber number We, Reynolds number Re, and contact angle $\theta = 15$ (measured value for clean glass) so that they can be directly compared with two published predictions (black line). Note that the square points correspond to prediction based on the left axis and the diamond points correspond to prediction based on the right axis.

accurate for a given number of terms. This approximation suggests that the extent that blood drop spreads follows:

$$\frac{r_f}{R} = \frac{We^{1/2}}{1.24 + We^{1/2}\,\mathrm{Re}^{-1/5}}. \qquad (2)$$

To compare the current experimental results with these previous model predictions, the Reynolds and Weber numbers were calculated using the impact velocity and drop size observed with high-speed camera along with the measured liquid properties (Section 2.2). Fig. 3c shows the predictions from the first model, Eq. (1), plotted with blue diamonds. The measured spreading factor corresponds to the horizontal axis and the predicted value corresponds to the right vertical axis. Similarly, the predictions from the second model, Eq. (2), are plotted with red squares so that the predicted values correspond to the left vertical axis. If the predicted measurements were the same as what was observed, these points would fall on the black line. Fig. 3c demonstrates that although these models are not identical, both predict the observed spreading factor within 10% of the clean glass experimental measurements.

3.2. Low impact bloodstains on microscopic coatings and residues

We next explore the bloodstains on all five surfaces in low impact conditions. The images taken one hour after impact show that when bloodstains formed on the various coatings they were remarkably different from those that formed on the clean glass (Fig. 4). A dotted circle with the size of the clean glass stain had been added to each image to highlight this difference. In these images, drops with 1-mm radius were released from $h = 20$ cm and drops with 2-mm radius were released from $h = 10$ cm. Because the impact velocity scales as $U \propto h^{1/2}$, doubling the height for the smaller drops leads to a similar Weber number for both drop sizes in the experiments, here approximately $We = 160$.

There are a few noteworthy features in these stains. Not only do the fingerprint and oil coatings lead to smaller bloodstains, but these stains are irregular and fragile. In particular, they more easily delaminate and fracture during drying. For the case of the half clean-half fingerprint coated glass, the bloodstain captures the asymmetry of the surface coating. On the clean half, the drop dries with the same shape and size as if it were on a fully clean surface. Whereas on the coated half, the bloodstain is more compact and shares similarities with those on the surfaces fully coated by oil and fingerprint residues. For the case of superhydrophobic coating, when the surface was flat, the blood dries as a beaded up drop, whereas when the surface was tilted by a small amount (7°), even less volume is left behind. Finally, a keen observer will note that a ring stain surrounds the principal stain for the larger drop on the fingerprint coated glass (Fig. 4, 2nd from left, bottom row). This ring is reminiscent of a coffee stain [35] and suggests that the contact line may have been temporarily stuck or pinned at that position as it dried.

Additional insight into how these final stains developed can be gained by evaluating images of the stains taken at both the millisecond and minute timescale. Fig. 5 shows a series of high-speed images taken at the time of impact for the larger drops that developed the stains in Fig. 4 (bottom row). Each column corresponds to a particular time t measured in millisecond relative to the time of impact ($t = 0$). Each row corresponds to a different surface with either a top-view perspective (Fig. 5a) or side-view perspective (Fig. 5b). The images show that the drops are spherical with a radius of $R = 2 \pm 0.1$ mm as they impact the surfaces at $U = 1.5 \pm 0.1$ m s^{-1}, leading to a Weber number of $We \approx 160$. The drops rapidly spread out, reaching a maximum radius of approximately $r_{max} = 6$ mm in approximately 5 ms. At this point, the flattened drop is thicker along its perimeter than center. For the blood drop on the clean glass, the drop stays at this size, but the thickness profile adjusts so that the thickness decreases from the center outward.

By contrast, on the fingerprint-coated surface, the drop begins to retract after reaching a maximum radius (Fig. 5). Indeed, on the half clean-half fingerprint substrate, the stain retracts only on the fingerprint-coated portion. A similar retraction is observed on the oil-coated glass. On the superhydrophobic surface, the retraction dynamics are so extreme, that the blood drop forms an upward jet within 25 ms after impact. When the superhydrophobic-coated glass is flat, the blood drop adheres to the surface and the drop returns to the surface intact. However, when the superhydrophobic surface is slightly tilted, the majority of the blood drop can bounce off of the impact spot within a fraction of a second, leaving only a small speck of blood behind (Fig. 5b). To be clear, these types of spreading and retraction dynamics after impact are well known for simple liquids, such as water [36,37].

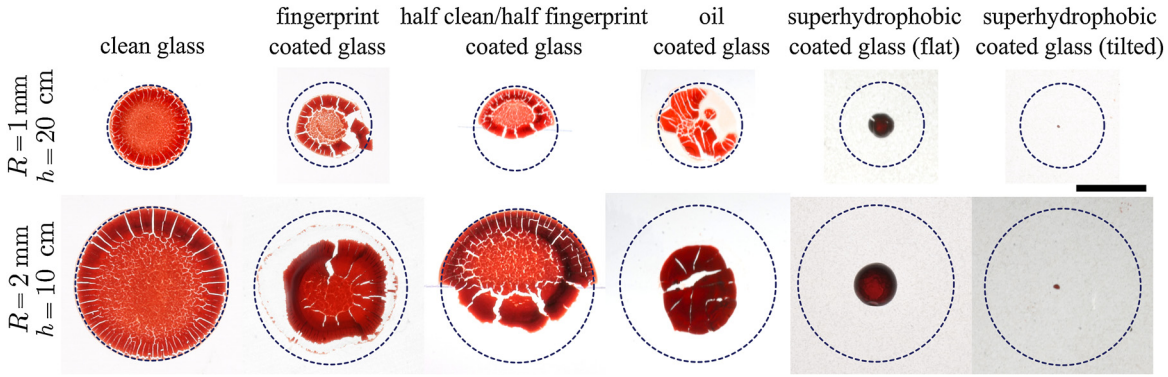

Fig. 4. Top-down view of the final dried bloodstains on the glass surfaces with the various coatings. Each row corresponds to the same set of impact conditions. The blue dotted circle was added to indicate the size of the stain relative to that on clean glass. All the glass surfaces were flat, except for the far right images, which were slightly inclined (7°). The scalebar of 5 mm applies to all images.

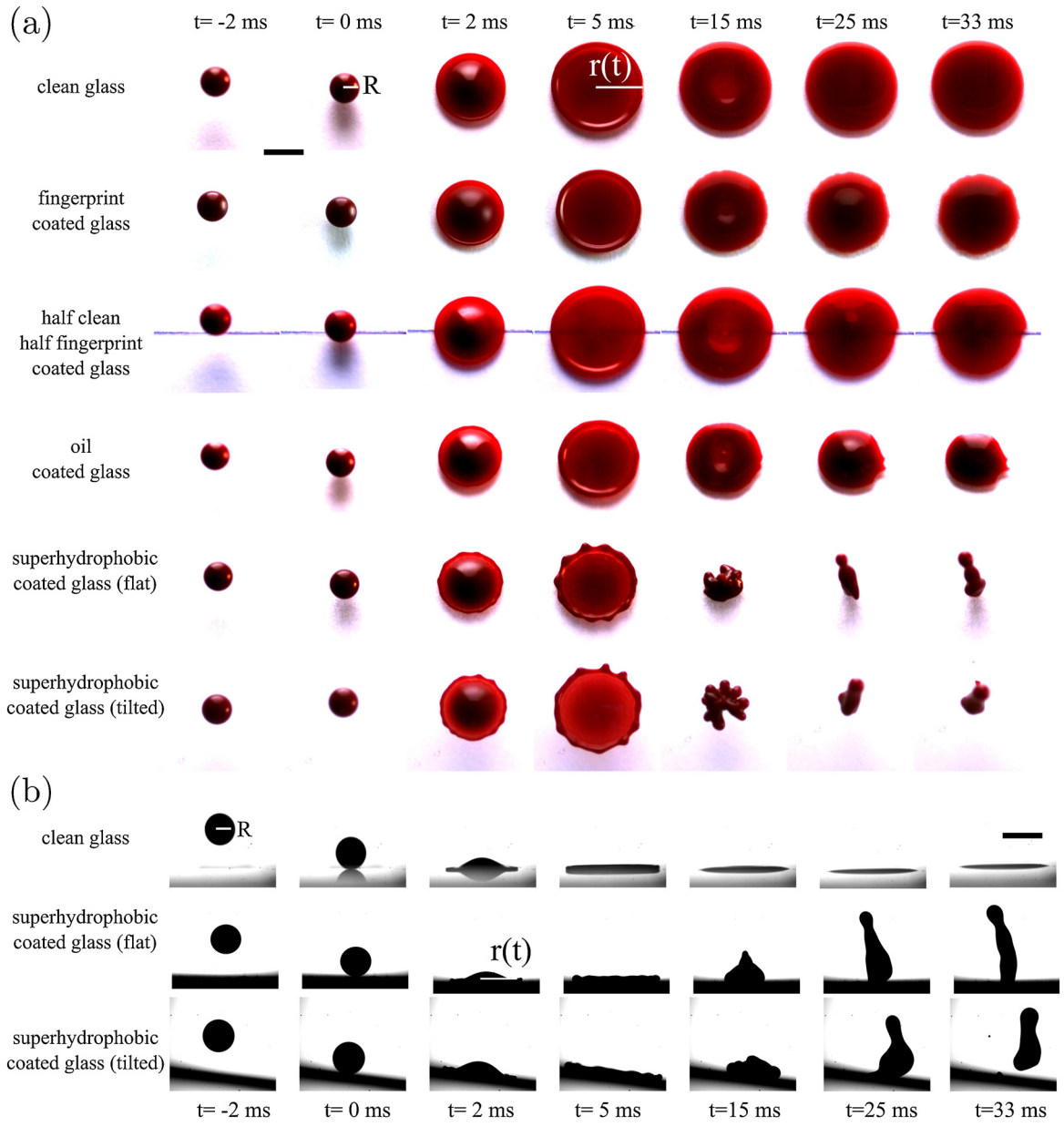

Fig. 5. High speed images of the initial impact dynamics of the blood drops. (a) A top view perspective illustrates how the contact radius r depends on time t and is affected by the various surface coatings. (b) Simultaneous images from the side view provide additional perspective. Here $R = 2.0 \pm 0.1$ mm and $U = 1.5 \pm 0.1$ m s^{-1}. The scalebar of 5 mm applies to all images.

What is less clear is their relevance to forensic science and the final configuration of a bloodstain.

To see how the coatings affect the longer-time stain formation, comparisons are made between the top-view images of the drops over timescales of minutes to hours (Fig. 6). Overall, the stain sizes and shapes do not appear to substantially change during the drying process. An exception occurs on the fingerprint-coated glass, as there appears to be a stick-slip dynamic between the images taken at 30 and 60 min. Specifically, the contact line for this drop suddenly retracts as the drop dries, leaving behind a faint ring of dried blood (Fig. 6, second row).

The drying dynamics on the clean glass is similar to what has been previously documented [38]. Within 10 min of being on the surface, the drop changes color as it solidifies and appears to form a thicker rim region. Within 30 min, the drop has completely dried, and cracks have formed along the rim. On the coated surfaces, the drop takes longer to completely dry, perhaps because it is thicker, as indicated by the darker color when backlit (Fig. 6).

Taken together, the short and long-time dynamics indicate that stain size on these microscopic coatings (Fig. 4) is predominantly set within the first tenth of a second. The early-time spreading and retraction can be quantified by measuring the contact radius r over time t. Fig. 7a plots this contact radius, normalized by the initial drop radius, for the drops illustrated in Fig. 5. Note that during the spreading phase, the dynamics are indistinguishable and the differences in the stain size appear to be related to the speed at which the extended droplet retracts. The final spreading factor β is also included for comparison. The retraction speed and timescale are consistent with a mechanism in which the contact lines recede to lower the surface energy while being resisted by the liquid inertia [39,40]. This mechanism indicates that the contact angle θ of the coating is likely an important parameter when predicting the final stain size. Recall

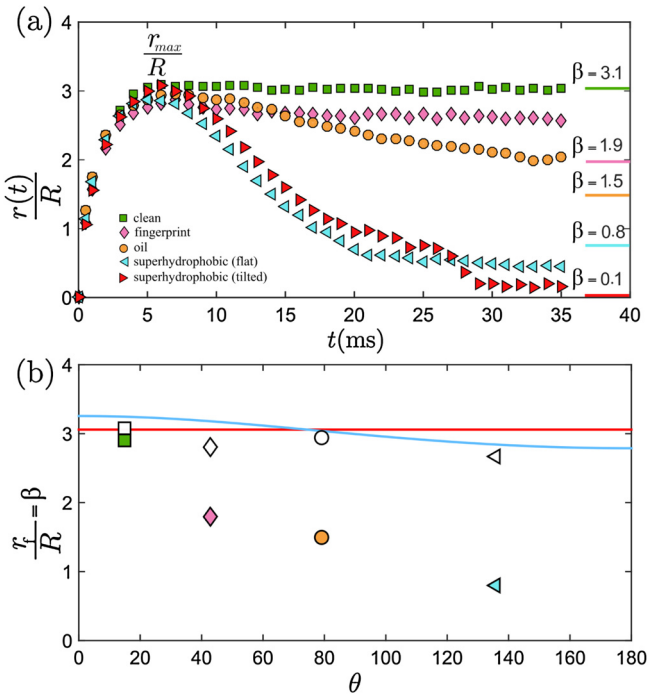

Fig. 7. Plot of the contact radius $r(t)$ and final spreading factor β for the blood drops depicted in Figs. 5 and 6 . (a) The normalized contact radius $r(t)/R$ spreads to a maximum value r_{max}/R ms after impact. Subsequently, the drop can recede and eventually reaches a final spreading factor β. (b) The final spreading factor $r_f/R = \beta$ depends on the measured contact angle θ of the coating (closed symbols) and is plotted along with the prediction from current theories (Eq. (1), blue line and Eq. (2), red line). The model is in closer agreement with the maximum extent that the blood spreads (open symbols) than the final stain size (closed symbols).

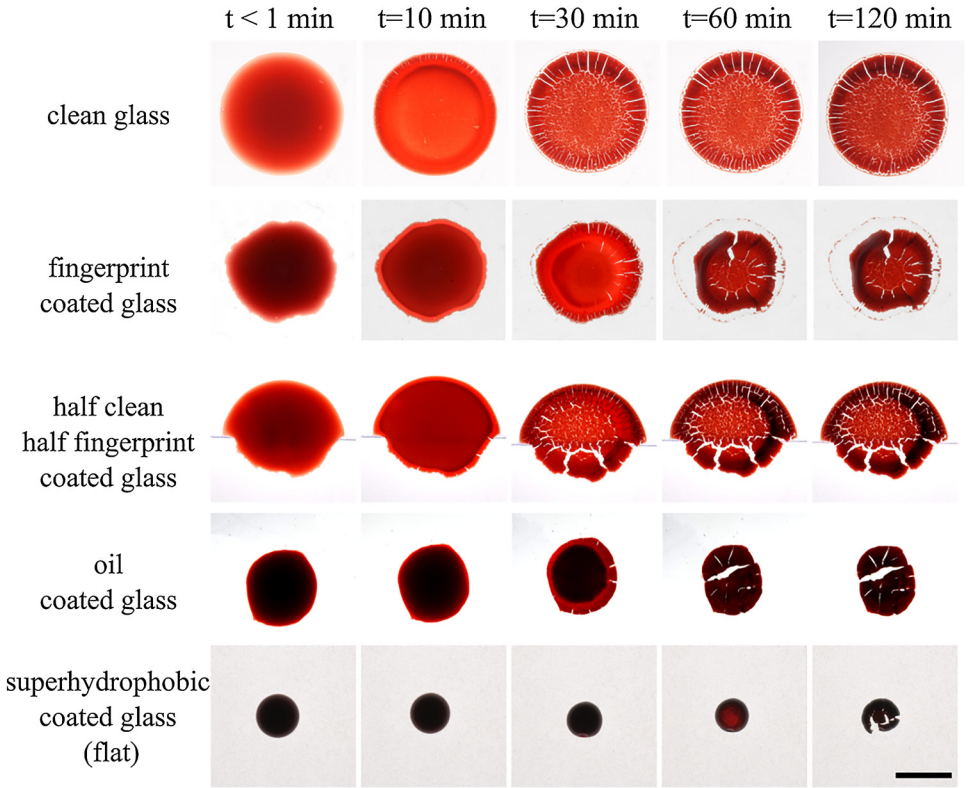

Fig. 6. Time series of the drying process for the blood drops depicted in Fig. 5. All drops were in their final configuration after 2 h. Note that the line visible in the half clean-half fingerprint binary coating is on the opposite side of the glass slide and used to identify the edge of the coating. The scalebar of 5 mm applies to all images.

that contact angles between each of the surfaces, blood, and air were measured and tabulated in Fig. 1b.

The spreading factor β of the blood stain decreased monotonically with increasing contact angle θ for the different microscopic coatings (Fig. 7b, closed symbols). Although this wettability measure is often neglected when predicting bloodstain size, it is included in some models, such as Eq. (1). Yet the influence of contact angle in the current results appears much greater than might be expected from this model. To illustrate this point, results from the models (the ones that adequately predicted the final stain size for the clean glass slides in Fig. 3c) are plotted alongside the data in Fig. 7b. Note that these models predict that the drop will spread out to approximately three times its initial radius for any contact angle. The bloodstain on the clean glass slide spreads out to this size, but the other flat coatings result in final stain diameters that are 35–72% smaller.

The primary source of discrepancy between these models and the current results is likely the tacit assumption that droplet spreads to a particular size and remains at this size as it dries. In other words, the final bloodstain size r_f is identical to its maximum size r_{max}. Had this constraint held for the current results and the final stain were the same as the maximum spreading radius, the spreading factor would have been much closer to the predictions (Fig. 7b, open symbols). It should be noted that this assumption is completely appropriate for the clean glass slide, and likely appropriate for other clean surfaces. Indeed, if this assumption was not made and the drops were completely free to adopt a final configuration that minimized energy, they would form spherical caps based on their initial size and contact angle. In this case, the spreading factor would be completely independent of the impact conditions and depend only on the surface conditions.

One reason why blood drops might stay at their maximum spreading size on a clean surface is that the contact line becomes pinned. It is well known that colloidal particle can jam at a contact line, preventing it from receding [41,42]. If this is the case, it makes the authors' choice of forensically-relevant coatings all the more noteworthy, as they prevent the blood drop contact line from pinning, at least initially. A reduction in contact line pinning is also consistent with a reduction in adhesion between the dried blood and the coatings. The dried blood on the oil-coated glass can be readily displaced and can completely detach from the superhydrophobic surface with a slight external force, such as a gentle breeze. The blood drops on the fingerprint-coated glass appears to have more adherence, but still noticeably less than on the clean glass surface.

3.3. High impact bloodstains on microscopic coatings and residues

It is natural to inquire whether the effects of the coatings that were observed at relatively low impact conditions (Fig. 7) extend to higher impact conditions as well. In particular, it is noteworthy that the impact conditions for the larger blood drop ($R = 2$ mm) released at $h = 100$ cm (impacting the surface at $U = 4.5 \pm 0.2$ m s^{-1}), are substantial enough for splashing to be expected [43], yet no clear evidence of splashing is observed for the stain on the clean glass surface (Fig. 3b).

Fig. 8 illustrates the final bloodstain configurations when the drops impact the various surfaces at this higher release height and directly compares them to the bloodstains released from the lower height. Here $R = 2.0 \pm 0.1$ mm and higher height leads to an impact velocity of $U = 4.5 \pm 0.2$ m s^{-1} and Weber number of $We \approx 1400$. The presence of the coatings has an even larger effect at this higher impact speed. The principle stain is smaller on the coated glass surfaces than on the clean glass and more irregular. Indeed on the oil-coated and superhydrophobic-coated glass, small droplets surround the principle stain (denoted with arrows in Fig. 8).

High-speed imaging of initial impact dynamics of these stains illustrates the drop on the clean surface spreads to a maximum size and the contact line remains pinned (Fig. 9). By contrast, the contact lines on the coated surfaces retract to varying degrees, similar to what was observed for the lower impact conditions. However, unlike what was observed for the lower impact conditions, the initial spreading of the high impact drops differs between the different coatings. In particular, spines and ligaments develop on the oil-coated and superhydrophobic-coated glass and breakup to form the tiny surrounding droplets (Fig. 9). On the superhydrophobic surface, holes nucleate in the center of the film as it begins to retract. As these holes expand, more ligaments are formed, although many of these recoalesce to form a principle drop.

Over the drying timescale, the drop shapes changes only slightly, with the exception again being the stain on the fingerprint-coated glass (Fig. 10). As the drop on the fingerprint-coated glass dries, the contact line appears to first stick and then slip, creating small flakes of dried blood that are loosely connected to the surface. The drops appear to fully dry within an hour. Fractures occur for the drops on the coated surfaces, which may be due to a combination of them being thicker and less well adhered to the surface.

The differences in the bloodstain sizes between the low and high impact conditions for the various coatings offers a way to

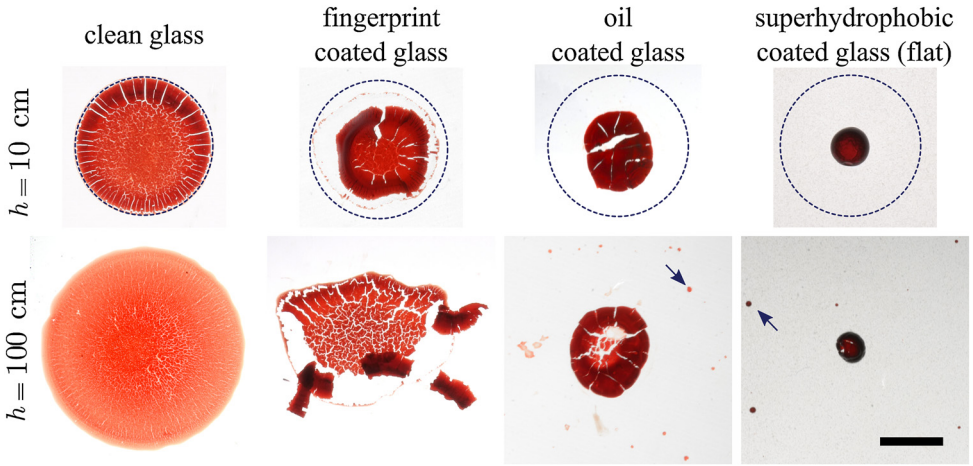

Fig. 8. Comparison of bloodstain patterns at lower and higher release heights h for the various coatings. The dried stains can develop highly irregular shapes, and numerous tiny droplets surround the principle stains on the bottom left two images (highlighted with arrows). Here the initial drop sizes are all the same with radius $R = 2.0 \pm 0.1$ mm and release heights are $h = 10$ and $h = 100$ cm. The scalebar of 5 mm applies to all images.

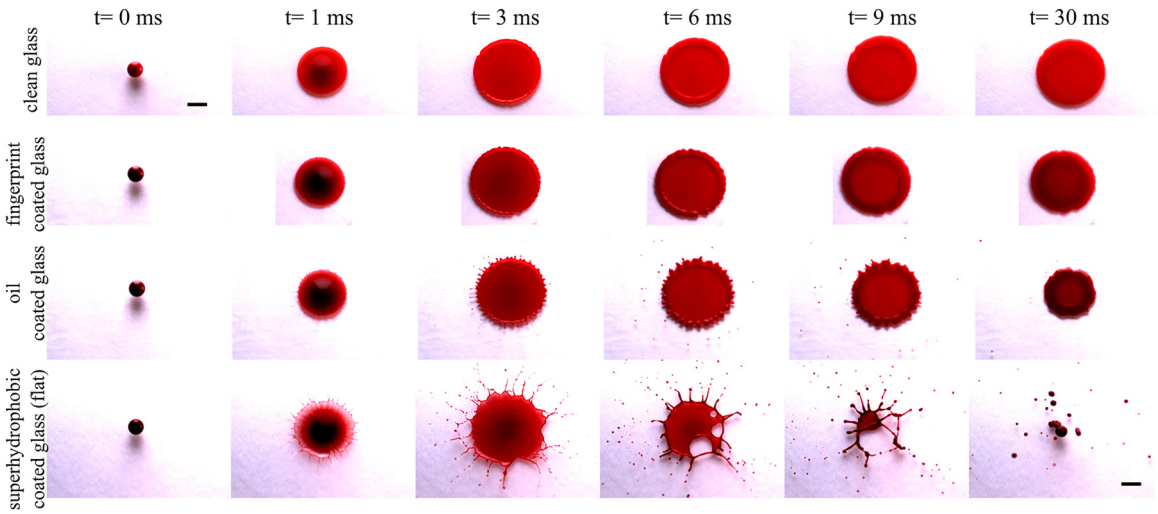

Fig. 9. High-speed images of the initial impact dynamics for the blood drops illustrated in Fig. 8. The top-view perspective illustrates how the surface coatings modify certain dynamics, such as crown splashing and spine formation, characteristic of the faster impact velocity. Here $R = 2.0 \pm 0.1$ mm and $U = 4.5 \pm 0.2$ m s^{-1} leading to a Weber number of $We \approx 1400$. The scalebar of 5 mm applies to all images.

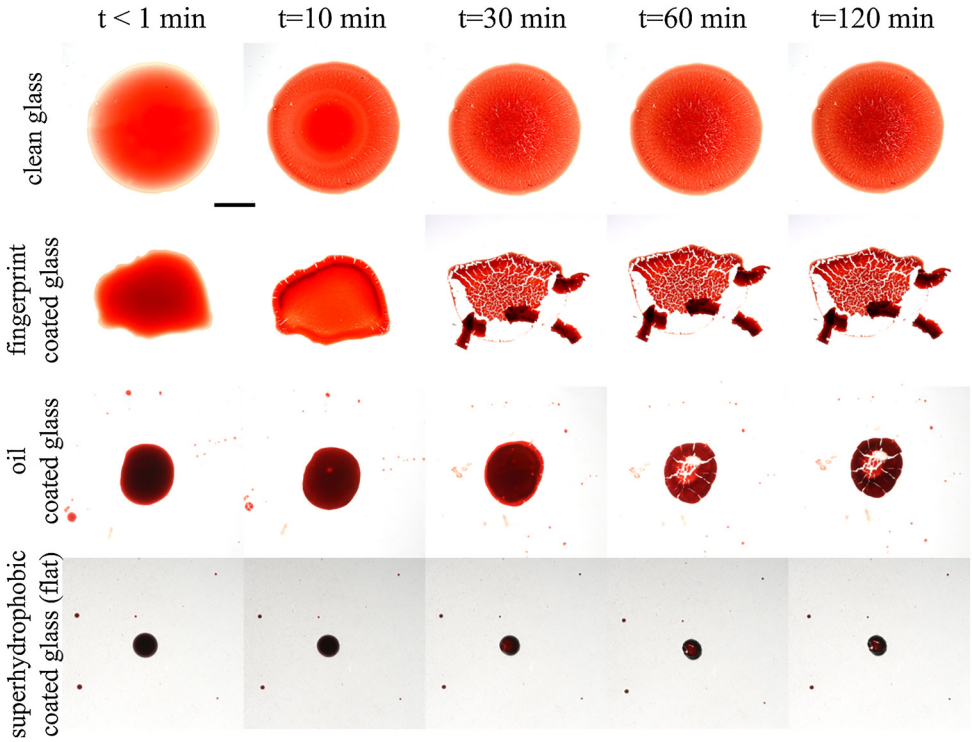

Fig. 10. Longer time dynamics of bloodstain drying process for blood drops depicted in Fig. 8. In all coated surfaces not only were the stains smaller than the clean surface, but drop spatter was observed around the primary stain. The scalebar of 5 mm applies to all images.

assess whether the ideas of contact line pinning in the last section continue to be consistent with the data. With the assumption that the contact line becomes pinned when the drop reaches its maximum extent, the higher impact velocity should lead to a larger stain, as illustrated with bloodstains on the clean glass (Fig. 8, first column). If no contact line pinning occurs, then the stain size should be independent of the impact velocity. This claim seems consistent with the size of the bloodstains on the oil-coated glass (Fig. 8, third column). Interestingly, the size of the stain on the fingerprint-coated surface increases with the impact velocity, but is smaller than the clean glass, suggesting a contact line pinning that is between the two extremes.

3.4. Role of clotting on bloodstains

The final section of this study explores whether the bloodstain configurations on the various coatings would be significantly modified if the blood were able to clot. Most laboratory experiments of bloodstains include anticoagulant to keep the blood from clotting between experiments; however, if the results are

significantly influenced by the presence of the anticoagulant, they would be less applicable to a crime scene where bloodstains can clot. To provide evidence that the results in this manuscript extend to blood that can clot, the anticoagulant is deactivated following the procedure outlined in Section 2.3 and the low impact experiments are repeated with $R = 2$ mm and $h = 10$ cm on the five surfaces (Fig. 11).

The final dried bloodstains demonstrated that the presence of these coatings noticeably reduced the size of the bloodstain relative to the clean glass regardless of whether the blood was able to clot. Given that the high-speed images indicate that most of the stain reduction occurs within a fraction of a second upon impact, it is not particularly surprising that clotting—which typically is associated with longer time periods—has a negligible effect. Nevertheless, there are some aspects of the bloodstains that differ between the activated and deactivated anticoagulant experiments that warrant closer inspection. In particular, the stain on the fingerprint-coated glass appeared to undergo a sudden retraction on the hour time-scale (Fig. 6). One might think that clotting might prevent the pinned contact line from retracting on this timescale, and indeed no evidence of a stick-slip condition is observed. Yet the size of the final stain is similar for the two anticoagulant cases (Fig. 11a, second column), suggesting the possibility that the blood did not pin on the finger-coated glass in the first place.

The notion that the contact line of the bloodstains with the deactivated anticoagulant are less likely to pin than with the activated anticoagulant is supported by additional stain features in Fig. 11. When the stain fragments, the fragments appear closer together when clotting can occur. Additionally, the small stain left on the tilted superhydrophobic surface vanishes with the deactivated anticoagulant. Multiple tests were done to demonstrate that this effect was repeatable. The high-speed images of the impact show that this drop completely detaches from the interface (Fig. 11b), demonstrating that it is possible for a drop of blood to impact a coated surface without leaving a visible trace.

A final curious discrepancy between the activated and deactivated anticoagulant bloodstains is the stain profile and crack pattern on the clean glass (Fig. 11a, first column). For the human blood with the activated anticoagulant, there is a rim surrounding the stain that is darker than the interior, suggesting that it might be thicker. Along this rim, there are regularly-spaced radial cracks. These crack patterns are similar to those described by Brutin et al. [38]. In contrast, the human blood with the deactivated anticoagulant has a rim that is lighter than the interior, suggesting that it might be thinner. Rather than form cracks at constant angles from the center, a single crack is observed at a constant radius. This observation suggests that the anticoagulant may fundamentally alter the drying process, which could have implications to blood drying studies beyond forensics. It is important to note, that the present evidence relies on experiments with blood that has been previously spiked with anticoagulant, which could potentially differ from fresh blood. Nevertheless, the presence of clotting itself does not appear to negate the results from this paper.

4. Conclusions

To investigate the effect of microscopic coatings on a bloodstain size and shape, systematic drop impact experiments were conducted using dual-view high-speed imaging and time-lapse photography. Three nearly invisible coatings were applied to glass slides: natural secretions of a fingerprint, vegetable oil and a superhydrophobic coating. In contrast to prior studies in which surface conditions were essentially immaterial to the staining process, the results of this study illustrate that the effects of these specific coatings on bloodstains can be dramatic. At low impact velocity, the stain size relative to the clean glass reduced by 35% for fingerprint coated glass, 49% for oil coated glass, and 72% for flat superhydrophobic coated glass. When the superhydrophobic coated glass was tilted slightly, the blood drop could leave the surface with a minuscule stain (96% reduction) or no stain at all. At the higher impact velocity, not only was the stain smaller than the clean surface, but drop spatter was observed around the primary stain. High-speed imaging revealed that size differences were largely due to drop receding dynamics within the first milliseconds of impact and suggests that these coatings may have prevented the stain from pinning to the surface at the point of maximum spreading. This reduction in contact line pinning appears to allow the stain to continue shrinking during the drying stage. When the anticoagulant in the human blood drops was deactivated to allow for clotting—a process likely to occur in actual crime-scene

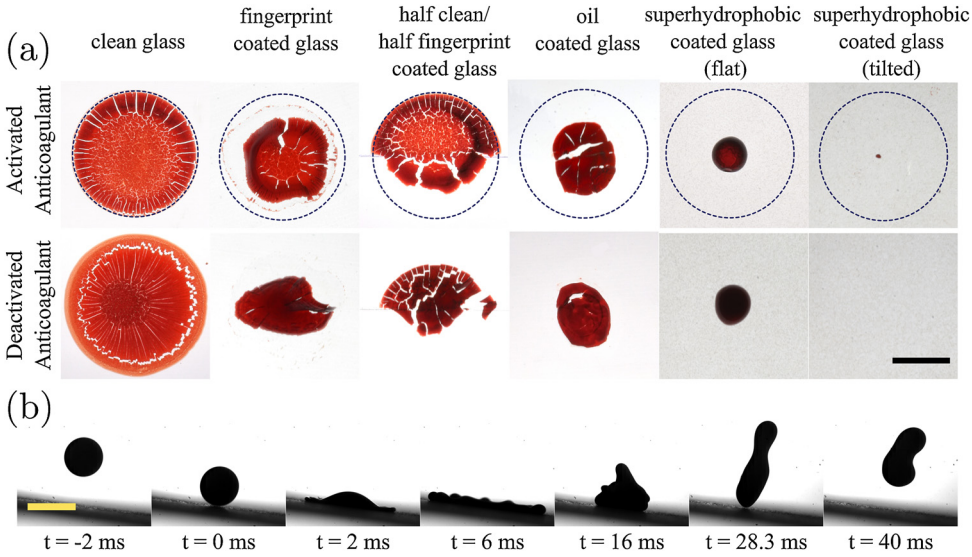

Fig. 11. Images illustrating the effect of blood clotting on the final stain pattern (a). Regardless of whether the anticoagulant is activated or deactivated, the coatings have a similar effect on the bloodstains. The conditions are identical to those in Fig. 4 bottom row (here repeated in top row for comparison). Note a few distinct differences that are repeatable and potentially significant—including the complete absence of a stain on the tilted superhydrophobic surface. (b) High-speed images of the blood drop, with the deactivated anticoagulant, completely bouncing off of the tilted superhydrophobic-coated glass and leaving no stain. The scalebar of 5 mm applies to all images.

situations—the results were similar to those for blood with active anticoagulant. Since the stain size and shape can be critical in conducting a bloodstain pattern analysis, our results highlight the need for forensic analysts to exercise caution when evaluating bloodstains on surfaces that might contain superhydrophobic coatings or oil residues, including latent fingerprint residue.

Author contributions

J.C.B. and K.F.M. conceived the research. S.S. designed and fabricated the experimental setup and carried out the experiments. S.S. and J.C.B. contributed to the development of the theory, conducted the analyses, and all the authors wrote the manuscript together.

Acknowledgements

The project was supported by the Boston University Dean's Catalyst Award. The authors thank Armela Murrizi for assistance in measuring blood viscosity.

Appendix A. Supplementary data

Supplementary data associated with this article can be found, in the online version, at https://doi.org/10.1016/j.forsciint.2018.12.008.

References

[1] P. Comiskey, A. Yarin, D. Attinger, High-speed video analysis of forward and backward spattered blood droplets, Forensic Sci. Int. 276 (2017) 134–141.
[2] R. Chen, L. Zhang, D. Zang, W. Shen, Blood drop patterns: formation and applications, Adv. Colloid Interface Sci. 231 (2016) 1–14.
[3] N.K. Osborne, M.C. Taylor, M. Healey, R. Zajac, Bloodstain pattern classification: accuracy, effect of contextual information and the role of analyst characteristics, Sci. Justice 56 (2) (2016) 123–128.
[4] U. Buck, B. Kneubuehl, S. Näther, N. Albertini, L. Schmidt, M. Thali, 3D bloodstain pattern analysis: ballistic reconstruction of the trajectories of blood drops and determination of the centres of origin of the bloodstains, Forensic Sci. Int. 206 (1–3) (2011) 22–28.
[5] M. Illes, M. Boué, Robust estimation for area of origin in bloodstain pattern analysis via directional analysis, Forensic Sci. Int. 226 (1–3) (2013) 223–229.
[6] C.R. Varney, F. Gittes, Locating the source of projectile fluid droplets, Am. J. Phys. 79 (8) (2011) 838–842.
[7] C. Knock, M. Davison, Predicting the position of the source of blood stains for angled impacts, J. Forensic Sci. 52 (5) (2007) 1044–1049.
[8] A. Carter, The directional analysis of bloodstain patterns theory and experimental validation, Can. Soc. Forensic Sci. J. 34 (4) (2001) 173–189.
[9] T. Bevel, R.M. Gardner, Bloodstain pattern analysis with an introduction to crime scene reconstruction, CRC Press, 2008.
[10] S.H. James, P.E. Kish, T.P. Sutton, Principles of bloodstain pattern analysis: theory and practice, CRC Press, 2005.
[11] K.G. de Bruin, R.D. Stoel, J. Limborgh, Improving the point of origin determination in bloodstain pattern analysis, J. Forensic Sci. 56 (6) (2011) 1476–1482.
[12] N. Laan, K.G. De Bruin, D. Slenter, J. Wilhelm, M. Jermy, D. Bonn, Bloodstain pattern analysis: implementation of a fluid dynamic model for position determination of victims, Sci. Rep. 5 (2015) 11461.
[13] L. Hulse-Smith, N.Z. Mehdizadeh, S. Chandra, Deducing drop size and impact velocity from circular bloodstains, J. Forensic Sci. 50 (1) (2005) JFS2003224-10.
[14] C.D. Adam, Fundamental studies of bloodstain formation and characteristics, Forensic Sci. Int. 219 (1–3) (2012) 76–87.
[15] C.D. Adam, Experimental and theoretical studies of the spreading of bloodstains on painted surfaces, Forensic Sci. Int. 229 (1–3) (2013) 66–74.
[16] N. Laan, K.G. de Bruin, D. Bartolo, C. Josserand, D. Bonn, Maximum diameter of impacting liquid droplets, Phys. Rev. Appl. 2 (4) (2014) 044018.
[17] S. Kim, Y. Ma, P. Agrawal, D. Attinger, How important is it to consider target properties and hematocrit in bloodstain pattern analysis? Forensic Sci. Int. 266 (2016) 178–184.
[18] M. Lettieri, M. Masieri, Surface characterization and effectiveness evaluation of anti-graffiti coatings on highly porous stone materials, Appl. Surf. Sci. 288 (2014) 466–477.
[19] G.E. Folk, A. Semken, The evolution of sweat glands, Int. J. Biometeorol. 35 (3) (1991) 180–186.
[20] J.W. Park, B. Vahidi, A.M. Taylor, S.W. Rhee, N.L. Jeon, Microfluidic culture platform for neuroscience research, Nat. Protoc. 1 (4) (2006) 2128.
[21] D. Richard, C. Clanet, D. Quéré, Surface phenomena: contact time of a bouncing drop, Nature 417 (6891) (2002) 811.
[22] S. Shiri, J.C. Bird, Heat exchange between a bouncing drop and a superhydrophobic substrate, Proc. Natl. Acad. Sci. U. S. A. (2017) 201700197.
[23] C. Willis, A.K. Piranian, J.R. Donaggio, R.J. Barnett, W.F. Rowe, Errors in the estimation of the distance of fall and angles of impact blood drops, Forensic Sci. Int. 123 (1) (2001) 1–4.
[24] F. Smith, C. Nicloux, D. Brutin, Influence of the impact energy on the pattern of blood drip stains, Phys. Rev. 3 (1) (2018) 013601.
[25] D. Attinger, C. Moore, A. Donaldson, A. Jafari, H.A. Stone, Fluid dynamics topics in bloodstain pattern analysis: comparative review and research opportunities, Forensic Sci. Int. 231 (1–3) (2013) 375–396.
[26] G.B. Thurston, Viscoelasticity of human blood, Biophys. J. 12 (9) (1972) 1205–1217.
[27] S. Chien, S. Usami, H.M. Taylor, J.L. Lundberg, M.I. Gregersen, Effects of hematocrit and plasma proteins on human blood rheology at low shear rates, J. Appl. Physiol. 21 (1) (1966) 81–87.
[28] E. Merrill, E. Gilliland, G. Cokelet, H. Shin, A. Britten, R. Wells Jr., Rheology of human blood, near and at zero flow: effects of temperature and hematocrit level, Biophys. J. 3 (3) (1963) 199–213.
[29] J. Andreas, E. Hauser, W. Tucker, Boundary tension by pendant drops, J. Phys. Chem. 42 (8) (1938) 1001–1019.
[30] T. Young, An essay on the cohesion of fluids, Philos. Trans. Royal Soc. 95 (1805) 65–87.
[31] R.J. Good, M. Koo, The effect of drop size on contact angle, J. Colloid Interface Sci. 71 (2) (1979) 283–292.
[32] M. Rånby, S. Ramström, P.-O. Svensson, T. Lindahl, Clotting time by free oscillation rheometry and visual inspection and a viscoelastic description of the clotting phenomenon, Scand. J. Clin. Lab. Invest. 63 (6) (2003) 397–406.
[33] L. Grunberg, A.H. Nissan, Mixture law for viscosity, Nature 164 (4175) (1949) 799.
[34] G.B. Foote, P. Du Toit, Terminal velocity of raindrops aloft, J. Appl. Meteorol. 8 (2) (1969) 249–253.
[35] R.D. Deegan, O. Bakajin, T.F. Dupont, G. Huber, S.R. Nagel, T.A. Witten, Capillary flow as the cause of ring stains from dried liquid drops, Nature 389 (6653) (1997) 827.
[36] A.L. Yarin, Drop impact dynamics: splashing, spreading, receding, bouncing, Annu. Rev. Fluid Mech. 38 (2006) 159–192.
[37] C. Josserand, S.T. Thoroddsen, Drop impact on a solid surface, Annu. Rev. Fluid Mech. 48 (2016) 365–391.
[38] D. Brutin, B. Sobac, B. Loquet, J. Sampol, Pattern formation in drying drops of blood, J. Fluid Mech. 667 (2011) 85–95.
[39] P.-G. De Gennes, F. Brochard-Wyart, D. Quéré, Capillarity and gravity, Capillarity and Wetting Phenomena, Springer, 2004, pp. 33–67.
[40] D. Bartolo, C. Josserand, D. Bonn, Retraction dynamics of aqueous drops upon impact on non-wetting surfaces, J. Fluid Mech. 545 (2005) 329–338.
[41] R.D. Deegan, O. Bakajin, T.F. Dupont, G. Huber, S.R. Nagel, T.A. Witten, Contact line deposits in an evaporating drop, Phys. Rev. E 62 (1) (2000) 756.
[42] B.M. Weon, J.H. Je, Self-pinning by colloids confined at a contact line, Phys. Rev. Lett. 110 (2) (2013) 028303.
[43] T.C. de Goede, N. Laan, K. de Bruin, D. Bonn, Effect of wetting on drop splashing of Newtonian fluids and blood, Langmuir 34 (18) (2018) 5163–5168.